Springtime transitions of NO_2, CO, and O_3 over North America: Model evaluation and analysis

Yunsoo Choi[1,2], Yuhang Wang[1], Tao Zeng[1], Derek Cunnold[1], Eun-Su Yang[1], Randall Martin[3,4], and Kelly Chance[4], Valerie Thouret[5], and Eric Edgerton[6]

Submitted to *J. Geophys. Res.*

November 21, 2007

[1]Georgia Institute of Technology, Atlanta, GA
[2]Now at Jet Propulsion Laboratory, California Institute of Technology, Pasadena, CA
[3]Dalhousie University, Halifax, NS B3H 3J5 Canada
[4]Harvard-Smithsonian Center for Astrophysics, Cambridge, MA
[5]Laboratoire d'Aerologie du CNRS, Toulouse, France
[6]Atmospheric Research and Analysis, Inc., Durham, NC

Corresponding author: Yuhang Wang, School of Earth and Atmospheric Sciences, Georgia Institute of Technology, Atlanta, GA 30332-0340. (Email: ywang@eas.gatech.edu)

Abstract

Surface observations from AIRNow and SEARCH networks, aircraft observations from the MOZAIC program, ozonesondes, and remote sensing measurements from GOME, TOMS and SAGE II for February-May 2000 over North America are used to characterize the springtime transitions of O_3 and its precursors. These measurements provide a comprehensive dataset to evaluate the performance of the 3-D Regional chEmical trAnsport Model (REAM). The model is then applied to analyze the key factors affecting the springtime transitions of trace gas concentrations and export. The global GEOS-CHEM model is used to provide chemical initial and boundary conditions. Generally, the model results are in good agreement with the observations in the troposphere except for a low bias of upper tropospheric O_3; the bias decreases towards the summer and lower latitudes. The rate of observed surface O_3 increase in spring is simulated by REAM. It is overestimated by GEOS-CHEM over the eastern United States. A key factor driving the model difference is daytime mixing depth. A shallow boundary layer in REAM leads to more efficient removal of radicals and hence slower activation of photochemistry in spring, when the primary radical source is relatively small. Comparison of top-down estimates of fossil fuel NOx emissions indicates the dependence of these estimates on model results. The associated uncertainty is up to 20% on a monthly basis. Averaging over a season reduces this uncertainty. While tropospheric column NO_2 decreases over the continent, it increases over the western North Atlantic due to lightning NOx production. Consequently the REAM model simulates significant increases of tropospheric O_3 over the region as indicated by column data derived from TOMS-SAGE II. Lightning impact is also evident in model-simulated NO_x exports.

1. Introduction

Ozone (O_3), carbon monoxide (CO), and nitrogen oxides (NOx = NO+NO_2), which are regulated under the National Ambient Air Quality Standards, are among the six criterion pollutants that adversely affect human health and biological ecosystems [NRC, 1991]. Ozone is a major precursor of the hydroxyl radical (OH), which plays a key role in oxidation chemistry in the troposphere. It is also a greenhouse gas, particularly in the upper troposphere. NOx and CO are major O_3 precursors produced during combustion. NOx is also emitted from soils and lightning, and CO can be produced during the oxidation of anthropogenic and biogenic hydrocarbons.

Springtime is a unique period to understand the behaviors of O_3 and its precursors over North America because of the rapid changes in the photochemical and dynamical conditions of the atmosphere. These changes are driven primarily by increasing solar insolation. The solar input energizes photochemical and meteorological processes directly by increasing radical sources through photolysis and the surface sensible and latent heat fluxes, respectively.

Meteorological changes are a powerful force that leads to changes in chemical processes. First, increasing water vapor due to warmer temperature increases the primary radical source through OH production from the reaction of $O(^1D)$ and H_2O, which results in more active photochemistry [e.g., Y. Wang et al., 2003a; Kondo et al., 2004]. Second, the abundance of water vapor and surface heating increase convection and lightning [Rind, 1998; Price, 2000], which is a large source of NOx in the free troposphere [e.g., Price et al., 1997]. Third, warmer surface temperature and precipitation increase NOx

emissions from soils [e.g., Yienger and Levy II, 1995]. One key atmospheric chemical species affected by all these processes is tropospheric O_3.

The Tropospheric Ozone Production about the Spring Equinox (TOPSE) experiment of 2000 was designed to measure tropospheric chemical changes during the spring transition period [Atlas et al., 2003]. The experiment took place from February to May 2000 over North America covering the region from Colorado to north of Thule, Greenland. These measurements were taken over remote regions at mid and high latitudes; in situ photochemistry [e.g., Cantrell et al., 2003; Y. Wang et al., 2003a] and large-scale transport of O_3 and its precursors to the measurement regions [e.g., Emmons et al., 2003; LaMarque and Hess, 2003; Y. Wang et al., 2003b; Allen et al., 2003; Y. Wang et al., 2006] are among the foci of previous TOPSE-related tropospheric chemistry analyses.

In this work, we explore the other aspects of tropospheric chemical changes during the spring transition periods, not covered by previous TOPSE-related analyses, using the rich datasets of in situ and satellite measurements available during the same time period over North America. In the process, we evaluate the Regional chEmical trAnsport Model (REAM). Certain aspects of this model have been evaluated in our previous applications of this model to analyze tropospheric chemistry and transport over the polar regions [Zeng *et al*., 2003, 2006; Y. Wang *et al*., 2007] and North America [Choi *et al*., 2005; Jing *et al*., 2006; Y. Wang *et al*., 2006; Guillas et al., 2007]. However, those evaluations lacked breadth because of the nature of the previous analyses. This is the first time that the evaluations of REAM model results with an extensive array of the observations are presented. For comparison purposes, selected results from the global

GEOS-CHEM model are used to illustrate key factors contributing to the observed features of springtime transitions of chemicals.

The springtime chemical changes provide a critical test for the simulation capability of REAM. The quality of the emission inventories strongly affects the model simulations of air quality. Emissions of NOx, in particular, are important for near-surface O_3 simulations. Satellite observations provide powerful constraints on surface NOx emissions [e.g., Martin et al., 2003]. We evaluate the model NOx emission inventory using satellite NO_2 measurements first. We further investigate the springtime transitions of different NOx sources. Second, we explore the changes of near-surface O_3, CO, and NOx concentrations during spring. Surface air quality changes are characterized from the observations of two monitoring networks, AIRNow by the U.S. Environmental Protection Agency (EPA) and the Southeastern Aerosol Research and Characterization Study (SEARCH). Third, we study the springtime changes of free-tropospheric O_3 as characterized by in situ measurements from the Measurement of Ozone and Water Vapor by Airbus In-Service Aircraft (MOZAIC) program and ozonesondes, and tropospheric column O_3 derived from the Total Ozone Mapping Spectrometer (TOMS) and the Stratospheric Aerosol and Gas Experiment (SAGE) II. Lastly, using the results of the REAM model, we examine the springtime exports of O_3 and its precursors from North America [e.g., Horowitz *et al*., 1998; Liang *et al*., 1998; Park *et al*., 2004].

We first describe the in situ and satellite measurements. The regional REAM and global GEOS-CHEM models are then described. After that, we examine the specific aspects of the springtime transitions of NOx, CO, and O_3. Conclusions are given in the end. In the appendix, we describe briefly the comparison of REAM simulations to

observed column CO by the Measurement of Pollution In The Troposphere (MOPITT) instrument.

2. Measurements

2.1 In situ measurements

EPA AIRNow network

Hourly O_3 concentrations are obtained from the EPA AIRNow data archives. The sites are divided into three categories: urban, suburban, and rural. The 291 rural sites are used since they are more representative of the region than urban sites. The detection limit value for O_3 was 5 ppbv. We focus on the afternoon (1300 to 1700 LT) when surface observations are more representative because of strong turbulent mixing in the planetary boundary layer (PBL). The CO and NOx measurements are not used because of their high method detection limits of 0.5 ppmv for CO and 5 ppbv for NOx (Jake Summers, Personal Comm., 2004). Rural CO and NOx measurements are usually below the detection limit values (reported as one-half the detection limit).

SEARCH network

Hourly O_3, NO, and CO are measured at eight SEARCH sites: Yorkville in Georgia (YRK, rural), Jefferson Street in Atlanta, Georgia (JST, urban), Centreville in Alabama (CTR, rural), Birmingham in Alabama (BHM, urban), Gulfport in Mississippi (GFP, urban), Oak Grove in Mississippi (OAK, rural), Outlying Landing Field #8 in Florida (OLF, suburban), and Pensacola in Florida (PNS, urban), For our analysis, we use observations from the following rural and suburban sites: YRK (85° W, 34° N), CTR (87° W, 33° N), OAK (89° W, 32° N), and OLF (87° W, 30° N). The detection limits of O_3, NO, and CO are 1 ppbv, 50 pptv, and 10 ppbv, respectively.

MOZAIC Program

The MOZAIC program was designed to automatically collect O_3 and water vapor data on five commercial Airbus A340 aircraft [Marenco *et al*., 1998]. For recent updates, see http://www.aero.obs-mip.fr/mozaic/. For the ascent and descent portions of the flights, MOZAIC raw data (4-sec time resolution) are averaged over 150-m height intervals. The MOZAIC analyzer is the dual-beam UV absorption Model 49-103 from Thermo Environment Instruments [Thouret *et al.,* 1998]. The instruments are laboratory-calibrated before and after flight periods and laboratory re-calibrated every 12 to 18 months. During flight operation, the instrument is automatically checked for zero and the calibration factor using a built-in O_3 generator.

Ozonesondes

We use ozonesonde data from six mid-latitude stations located between 35° and 53°N: Goose Bay (53°N, 50°W), Richland (46°N, 119°W), Trinidad Head (41°N, 124°W), Boulder (40°N, 105°W), Wallops Island (38°N, 75°W), and Huntsville (35°N, 87°W). The electrochemical concentration cell (ECC) sensor is typically used and the accuracy is about ±6% on the ground and -7% to 17% in the middle and upper troposphere [Komhyr *et al.,* 1995].

2.2 Satellite measurements

Tropospheric NO_2 vertical column from GOME

The GOME instrument is on board the European Remote Sensing-2 (ERS-2) satellite that passes over the equator at 1030 AM local time (LT), and its typical horizontal resolution is 40 km (along track) by 320 km (cross track). The retrieval algorithm and air mass factor calculation are described in detail by Chance *et al.* [2000]

and Martin *et al.* [2002]. First, the NO_2 slant column is determined by fitting directly backscattered radiance spectra measured by GOME. Then the stratospheric column determined from the NO_2 column over the central Pacific [Martin *et al.,* 2002] is subtracted from the total column. Finally, the subtracted columns are converted to vertical columns using air mass factors, which are an integral of the product of the shape factor from model-calculated vertical profiles and the sensitivity of backscattered radiance to NO_2. The radiance perturbation due to the change of NO_2 is calculated from the Linearized Discrete Ordinate Radiative Transfer (LIDORT) model [Spurr *et al*., 2001], which considers multiple scattering in the atmosphere. Data of cloud optical depth and fraction are from GOME [Kurosu *et al.,* 1999]. The monthly mean fields of aerosol mass concentrations are taken from the Global Ozone Chemistry Aerosol Radiation and Transport (GOCART) model [Chin, 2002], which simulates 3-D distributions of sulfate, mineral dust, sea salt, black carbon, and organic carbon. We do not use GOME measurements when cloud cover is >40% [Martin *et al*., 2002]. The retrieval uncertainties are mostly due to spectral fitting, spectral artifacts related to the diffuser plate, removal of the stratospheric column, and air mass factor calculations [Martin *et al.,* 2002; Choi *et al.,* 2005]. The uncertainties are generally $0.6\text{-}1.2\times10^{15}$ molecules cm^{-2} over the ocean and $1.0\text{-}3.5\times10^{15}$ molecules cm^{-2} over the continent.

Tropospheric O_3 column from TOMS and SAGE II

TOMS on board the Earth Probe satellite that crosses the equator at 1116 AM local time measures incident solar radiation and backscattered ultraviolet sunlight. Total atmospheric O_3 columns have a horizontal resolution of 39×39 km^2 with a measurement uncertainty of about 5%. SAGE II on board the Earth Radiation Budget Satellite (ERBS)

measured the Earth limb extinction via the solar occultation technique during each spacecraft sunrise and sunset. The horizontal and vertical resolutions of SAGE are about 30×250 km^2 and 1 km, respectively. Scatter-plots of SAGE II (retrieval version 6.2) O_3 versus potential vorticity (PV) on isentropic surfaces are used to produce the O_3 profiles in the stratosphere [Jing *et al.,* 2004], which are coincident in latitude, longitude, and time with TOMS (version 8) total column O_3 measurements. When the TOMS data indicate a reflectivity < 20%, tropospheric O_3 columns are inferred by subtracting the SAGE II-based stratospheric from the TOMS columns. The PV values are obtained from the NCEP reanalysis data set, and a value of 3.5 PV units is used to define the location of the tropopause.

By comparisons with the ozonesonde measurements, two previous studies [H-J. Wang *et al.,* 2002, 2006] indicate that SAGE O_3 has an accuracy of 10% or better down to the tropopause and that the SAGE data are 5% higher than the ozonesonde values at 15 -20 km. The PV-mapped SAGE O_3 column estimates between 340 and 800 K isentropic surfaces (~10-30 km) have a 4% error, compared to the ozonesonde observations at 30-60° N. Considering that 90% of total column O_3 resides in the stratosphere, the uncertainty of the derived tropospheric column O_3 is ~40%. The uncertainty is expected to decrease when tropospheric columns are averaged over a period of a month. In our analysis, we focus more on the qualitative aspects of model results in comparison to TOMS-SAGE II tropospheric O_3 columns.

3. Model Descriptions

In this work, REAM has a horizontal resolution of 70 km with 23 vertical layers reaching 10 hPa, 20 of which are below 100 hPa. The National Center for Atmospheric

Research/Penn State MM5 is used to simulate meteorological fields using four-dimensional data assimilation (FDDA) [Stauffer *et al*., 1991] based on the National Center for Environmental Prediction reanalysis, surface, and rawinsonde observations. Most of the meteorological variables are archived every 30 minutes, except those for convection and lightning which are archived every 2.5 minutes because of the highly variable nature of these processes. The horizontal domain of MM5 has five extra grids on each side of the REAM domain to minimize potential transport anomalies near the boundary. We use the ETA Mellor-Yamada-Janjic (MYJ) 2.5-order closure scheme [Black, 1994] for turbulence calculations. Regional simulations are spun up in the last week of January 2000.

The photochemical, dry, and wet deposition modules of REAM are adopted from the GEOS-CHEM model [Bey *et al.,* 2001]. The altitude-dependent cloud optical depth is calculated using MM5 liquid water content [Stephens *et al*., 1978]. The UV surface albedo distribution, for photolysis rate calculations, is obtained from TOMS observations [Herman and Celarier, 1997]. The transport scheme is from Walcek [2000]. The convective scheme by Grell [1993] is implemented to be consistent with the meteorological model; sub-grid scale updraft and downdraft processes and large-scale subsidence are considered. The top and bottom layers of shallow convection are determined by MM5 simulations; the cloud fraction is determined using the scheme described by Geleyn [1981].

Emission inventories for combustion and industrial sources are taken from GEOS-CHEM [Bey *et al*., 2001], except the fossil fuel NOx and CO emission inventories over the United States, which are taken from the 1999 US Environmental Protection Agency

National Emission Inventory. These values are scaled with the national total emissions of 2000 [EPA, 2003]. Emission algorithms for vegetation and soils are adopted from GEOS-CHEM, although meteorological inputs are from MM5. Parameterizations of NOx from lightning as functions of convective mass flux and convective available potential energy are the same as described by Choi et al. [2005].

Spring 2000 GEOS-CHEM model simulations provide initial and boundary conditions for trace gases. GEOS-CHEM (version 7.2) is driven by GEOS assimilated meteorological fields (GEOS-3) for 2000. The horizontal resolution of GEOS-CHEM is 2° latitude by 2.5° longitude. Detailed algorithms for photochemistry, dry and wet deposition, and emissions, many of which are adopted in REAM as discussed above, are described by Bey *et al*. [2001]. Algorithms of NOx emissions from lightning based on cloud top height by Price and Rind [1994] and from soils by Yienger and Levy [1995] were adapted by Wang et al. [1998].

4. Surface emissions of fossil fuel NOx

4.1 Dependence of GOME NO_2 retrievals on the a priori profiles

GOME NO_2 measurements provide useful constraints on surface NOx emissions [e.g., Martin et al., 2003]. The retrieval process is described in Section 2.2. To obtain the tropospheric vertical columns, model profiles of NO_2 are used to calculate the air mass factor. As a result, some model dependence of the retrieval is therefore convoluted in the retrieved vertical columns. As will be discussed in the next section, REAM and GEOS-CHEM models simulate different vertical profiles of tropospheric NO_2 (to be shown in Figure 6). We therefore compute the air mass factors separately from these two model results as a way of examining the sensitivity of GOME retrievals to the simulated NO_2

vertical profiles. Figure 1 shows good agreement between GOME NO_2 column retrievals using the REAM and GEOS-CHEM profiles between February and May 2000. The correlation coefficient is > 0.99. The monthly mean NO_2 columns of the retrievals using REAM profiles are higher by 6.1, 12.0, 5.5, and 0.4% from February to May than those using GEOS-CHEM profiles. Generally, a value of 15% is estimated as the NO_2-profile associated retrieval uncertainty [Martin *et al*., 2002], which encompasses the range of model derived difference found here.

4.2 Characterizations of tropospheric column NO_2

GOME derived tropospheric NO_2 columns in Figure 1 shows a decreasing trend over the continental region, particularly over high emissions regions in the Northeast and Midwest of the United States. In contrast, there is a clear increasing trend over the western North Atlantic. Comparing the two model simulations to the retrieved column NO_2, the mean biases are within 11%, and the correlations are high (R>0.85). Over the continent, the two models show similar trends as observed. The decreasing trend simulated in the model is driven by more active photochemistry as spring progresses towards summer. As a result, more NO_2 is removed by the reaction of OH and NO_2. Due to its coarse spatial resolution, the GEOS-CHEM model fails to capture high NO_2 columns ($>5\times10^{15}$ molecules cm^{-2}) in California, which are shown in REAM results. In April and May, both models slightly underestimate NO_2 columns in the western United States probably due to underestimated soil NOx emissions [e.g., Martin *et al*., 2003; Bertram *et al*., 2005]. While REAM tends to slightly overestimate GOME NO_2 columns in May partly due to larger lightning NOx productions, GEOS-CHEM tends to underestimate.

The large increase of column NO_2 over the western North Atlantic, despite increasing photochemical removal as the season progresses is captured by REAM. In comparison, no significant changes are shown in GEOS-CHEM simulations, leading to underestimates of column NO_2 in the region. We discuss the contributions of several factors to tropospheric column NO_2 in the next section.

4.3 Contributions of lightning, soil emissions, and convection to column NO_2

We compute the contributions of lightning production, convective transport, and soil emissions in the model by comparing the standard REAM simulation against simulations with one of these processes turned off. Figure 2 shows monthly mean column differences between the standard and sensitivity simulations. In February and March, lightning NO_2 enhancements are typically $<3.0\times10^{14}$ molecules cm^{-2}, but in April and May, they increase to $0.5\text{-}2.0\times10^{15}$ molecules cm^{-2} over the southern United States, the Gulf of Mexico, and the western North Atlantic. Typical monthly mean uncertainties for GOME retrievals are $2\text{-}9\times10^{14}$ molecules cm^{-2} over ocean, which is 20%-70% of typical uncertainties over the continent. Large enhancements from lightning and soil emissions simulated in May are larger than the retrieval errors on a monthly mean basis.

The lightning and soil emission contributions over land increase to about 10 and 7% of tropospheric column NO_2, respectively, in May. The estimated contribution of lightning is larger than that of soil emissions, except in February. The springtime increase of tropospheric column NO_2 over the western North Atlantic is driven by lightning NOx emissions in the REAM simulations. The increasing trend is not simulated by GEOS-CHEM because the algorithm by Price and Rind [1994] gives very low flash rates over the ocean.

4.4 Top-down estimates of fossil fuel NOx emissions

Optimized NOx emissions are estimated by combining top-down NOx emission estimates from satellite measurements with a priori bottom-up emissions, weighted by relative errors for the two estimates [Martin *et al*., 2003]. Both REAM and GEOS-CHEM use the same EPA 1999 NEI inventory for surface fossil fuel NOx emissions in the United States as the a priori.

The top-down NOx fossil fuel emission inventory (E_t) is first calculated following Martin *et al*. [2003] by fitting E_t to a priori bottom-up emission E_a with the ratio of the retrieved NO_2 column (Ω_r) to the simulated column (Ω_s):

$$E_t = E_a \times \Omega_r / \Omega_s \,. \qquad (1)$$

Monthly a posteriori emissions (E) are then calculated by the weighted averages of E_a and E_t [Martin *et al*., 2003]:

$$\ln E = \frac{(\ln E_t)(\ln \varepsilon_a)^2 + (\ln E_a)(\ln \varepsilon_t)^2}{(\ln \varepsilon_a)^2 + (\ln \varepsilon_t)^2} \,, \qquad (2)$$

where ε_a and ε_t are the a priori inventory and top-down emission errors, respectively.

Table 1 shows the monthly a priori, top-down, and a posteriori emissions derived using REAM and GEOS-CHEM results, respectively. The a priori emissions from REAM and GEOS-CHEM are almost the same, but the top-down estimates sometimes differ significantly. The top-down emissions derived by REAM are larger by 3% to 16% than those of GEOS-CHEM between February and April, and are smaller by 20% than GEOS-CHEM in May. Two sources contribute the variations in the top-down estimates. One is due to the difference in model simulated vertical profiles of NO_2 and hence the calculated air mass factors discussed in section 4.1. The other is the difference in model

simulated emission-column relationship used in Equation (1). For comparison, the standard deviation of monthly averages from the 4-month average is 16-19% in the each model, comparable to the difference between the two model estimates for each month. Therefore, time averaging (> 1 month) is needed to derive a more robust top-down estimate. On a seasonal basis, the top-down and a posteriori emissions are almost exactly the same as the a priori.

5. Spring transitions of near-surface air quality

Springtime air quality changes can be characterized by the measurements from the EPA AIRNow monitoring network. To avoid the problems in the reported CO and NOx measurements from this network (section 2.1), we first make use of the measurements of NO, CO, and O_3 from the SEARCH networks, even though the geographic coverage of the SEARCH dataset is limited.

5.1 Spring trends of NO, CO, and O_3 at SEARCH sites

Inspection of NO, CO, and O_3 concentrations at the four SEARCH rural sites (CTR, OAK, OLF, and YRK, section 2.1) in February-May 2000 reveals that these sites show similar multi-day temporal patterns (not shown), which are driven by synoptic-scale meteorological changes over the region. To illustrate the comparison, we show the results at the OAK site in Figure 3. Hourly NO concentrations vary significantly between day and night because of the shallow boundary layer at night. We show only daily 1-5 pm (LT) values for NO. The temporal variation pattern is not well characterized by NO concentrations even though that periods with elevated NO at all four sites can be found. The model has some capability to capture the NO variations. The multi-day synoptic-

scale variations are better characterized by CO and O_3, which have longer chemical lifetimes. These variations are simulated by the model.

The correlations coefficients between REAM and SEARCH NO are higher at CTR and OAK sites (0.66 and 0.56, respectively) than OLF and YRK sites (0.40 and 0.23, respectively). The lower correlations at the latter two sites reflect the coastal location of the OLF site and the large influence of power plant emissions at the YRK site. The model resolution is too coarse to simulate properly the influence of power plant plumes. The correlation coefficients for CO are in the range of 0.52-0.63 except the YRK site (0.48). Too much influence from CO emissions in Atlanta is simulated in the model because the proximity of Yorkville to Atlanta (60 km). The correlation coefficients for O_3 are in the range of 0.65-0.69.

The seasonal transitions of NO, CO, and O_3 are different. Concentrations of NO decrease, reflecting in part the increasing photochemical loss of NOx. The trend is consistent with GOME measurements (Figure 1). The seasonal decrease of CO is relatively small during spring. Increasing CO loss due to increasing OH oxidation is compensated for by faster CO production from VOC oxidation. Ozone, in comparison, clearly has an increasing trend as photochemistry becomes more active. These trends are simulated well by REAM. We also compared GEOS-CHEM simulations with these surface observations (not shown). One large difference between REAM and GEOS-CHEM is that GEOS-CHEM tends to overestimate surface O_3 concentrations in April and May. We look at this issue using the measurements from the AIRNow network, which has good spatial coverage over the contiguous United States.

5.2 Surface O_3 increase in AIRNow measurements

Monthly mean afternoon (1300-1700, LT) O_3 concentrations measured by the EPA AIRNow surface sites are compared with REAM and the GEOS-CHEM simulations from February to May (Figure 4). High O_3 peaks are captured by REAM to within 10 ppbv. The correlation coefficients of the REAM and GEOS-CHEM results with the measurements are in the range of 0.56-0.65 and 0.44-0.68, respectively. The correlations between the GEOS-CHEM and AIRNow observations decrease as the season progresses towards summer while the opposite is true for REAM.

As the season processes towards summer, increasing solar influx and water vapor activates photochemistry [e.g., Y. Wang *et al.*, 2003]. Both REAM and GEOS-CHEM simulate the resulting increase in surface O_3. The rates of photochemical activation and surface O_3 increases are better simulated in REAM than in GEOS-CHEM. The global model simulates higher O_3 concentrations over the eastern United States in April and May than AIRNow observations. Inspections of the model difference between REAM and GEOS-CHEM reveal that a major contributing factor is the differences in the boundary layer mixing depth used in the models.

5.3 *Daytime mixing depth and surface O_3*

It was known that mixing depth of the boundary layer affects surface O_3 concentrations [e.g., Holzworth, 1964, 1967]. From February to May, both MM5 and GEOS-3 predict increasing boundary layer mixing depth as solar insolation increases (Figure 5). However, MM5 predicted mixing depths (used in REAM) are in general lower than GEOS-3 predictions (used in GOES-CHEM). The difference is particularly large over the eastern United States, where the difference is up to a factor of 2.

Unfortunately routine meteorological observations do not provide useful information to evaluate model simulated afternoon mixing depth.

The shallower mixing depth in REAM results in stronger boundary layer vertical gradients and higher surface concentrations of CO and NOx but lower concentrations of O_3 than GEOS-CHEM over the eastern United States (Figure 6). The effect of boundary layer mixing is best demonstrated by CO distributions since its photochemical source is relatively small compared to emissions and its lifetime is long. Below 900 hPa, REAM simulates higher concentrations than GEOS-CHEM. The opposite is true between 700-850 hPa, reflecting more efficient mixing in GEOS-CHEM. From March to May, the REAM-GEOS-CHEM difference of CO near the surface increases, reflecting a faster mixing depth increase in GEOS-CHEM than REAM. Similar characteristics are found for NOx and O_3. Surface CO and NOx are larger by ~50 ppbv and ~1 ppbv, respectively, in the REAM results. In contrast, REAM surface O_3 mixing ratios are lower by 5-10 ppbv. REAM simulated increase of NOx concentrations in the upper troposphere, particularly in May, is due to lightning NOx production.

During spring, the radical source, which is largely driven by photon flux and water vapor [e.g., Y. Wang *et al*., 2003], is limited. High concentrations of NOx decrease photochemical activity because of increasing radical loss through the reaction of OH and NO_2. Thus, less active mixing in REAM results in lower surface O_3 production and concentrations than GEOS-CHEM during spring, leading to better agreement with AIRNow surface measurements (Figure 4).

6. Free-tropospheric O_3 in spring

6.1 In situ O_3 measurements

We first examine in Figure 7a the vertical O_3 profiles from ozonesondes and MOZIAC program during spring. MOZAIC profiles are taken during takeoff and landing from cities including Toronto, New York City, Chicago, Washington DC, Atlanta, Houston, and Dallas. Most of the data are over the eastern United States because the measurements were made on commercial flights between the United States and Europe. Model results are in good agreement with the measurements in the lower and middle troposphere, except for a low bias of 10 ppbv at Wallops Island. The site is located at a baroclinic zone with large O_3 gradients [Thouret *et al*., 2006], making it more difficult to simulate in the model. The boundary-layer O_3 trend in spring was discussed in section 5. We investigate the seasonal O_3 trend in the free troposphere (400-800 hPa.) in Figure 7b. Ozonesonde and MOZAIC measurements show an increase of ~10 ppbv from February to May. This magnitude of increase is captured well by REAM, although REAM monthly mean mixing ratios are lower than the measurements by ~3 ppbv.

In the upper troposphere, however, the REAM model has a clear tendency to underestimate. To illustrate the spatial and temporal distributions, we show in Figure 8 a comparison of MOZAIC measurements with REAM results at 150-250 hPa from February to May. MOZAIC measurements have better data coverage in this region than lower altitudes because it is close to the cruise altitude of aircraft. We filtered out mixing ratios > 200 ppbv in the measurements (and model results) to minimize the effects of extreme values.

In general, REAM tends to underestimate O_3 concentration measurements. Thouret *et al*. [2006] found that spring maximum O_3 in the MOZAIC measurements is located in the lower stratosphere, where O_3 concentrations range from 150 to 500 ppbv

with a strong vertical gradient near the tropopause region. The upper tropospheric O_3 simulations in REAM are strongly affected by the specified upper boundary conditions at 100 hPa from GEOS-CHEM, which exhibits difficulties in simulating the sharp O_3 gradient across the tropopause [Bey *et al*., 2001]. REAM results in the upper troposphere improve towards May as tropospheric photochemical production contributes more to upper tropospheric ozone. In the same vein, Figure 7a shows that model low bias improves significantly as we move towards the lower-latitude sites or cities, where photochemical production of ozone is more active.

6.2 TOMS-SAGE II tropospheric column O_3

Ozonesonde and MOZIAC data do not provide enough coverage to allow examination of the spatial distribution of the spring increase of tropospheric ozone. We use the tropospheric column O_3 derived from TOMS and SAGE II measurements (section 2.2) here to qualitatively examine the seasonal transition in tropospheric O_3 columns. Figure 9 compares TOMS-SAGE II tropospheric O_3 column with REAM and GEOS-CHEM results from February to May 2000. The satellite products and the models show a springtime increase in tropospheric O_3 over North America, even though the absolute amounts of column O_3 derived from TOMS and SAGE II do not agree well with either model. High O_3 columns are clearly shown over the western North Atlantic in the satellite-derived columns, particularly in May. REAM produces significant enhancements over the region while GEOS-CHEM does not. A sensitivity REAM simulation without lightning NO production exhibits much weaker enhancements, suggesting that lightning NO production is a large contributor to O_3 enhancements over the western North Atlantic. While simulated lightning NOx enhancements cover a broad region (Figure 1), the

resulting O_3 enhancements are mainly in the southern region, where solar insolation is large and photochemistry is active.

7. Pollutant import and export

7.1 Vertical profiles of pollutant fluxes

Fluxes of NOx, NO_y, CO, and O_3 imported to and exported from the troposphere over North America are estimated using REAM. Fluxes through the western and eastern boundaries are a factor of 18 larger than through the north and south boundaries. Here, we focus on longitudinal fluxes. Figure 10 shows the vertical profiles of longitudinal import and export fluxes of these pollutants. While the export (in the eastern boundary) of CO decrease, exports of NOx and NOy show increases. The large increase of NOx in the upper troposphere is driven primarily by lightning NOx production. For example, simulated NOx export fluxes at 12 km increase from 1.8×10^7 moles day^{-1} to 4×10^7 moles day^{-1} from February to May. Sensitivity studies (not shown) indicate that lightning production enhances NOx and NO_y exports in the upper troposphere (8-12 km) by 250% and 66%, respectively, in May. Lightning NOx is oxidized to longer lived NOy species, which have longer lifetimes. Therefore the vertical gradient of NOy export is much less that of NOx. The decrease of CO export is associated in part with much longer lifetimes of CO during winter, allowing for the accumulation of CO at mid and high latitudes. As oxidation becomes more active spring, tropospheric CO concentrations begin to decrease; both export and import fluxes decrease. Ozone export in the upper troposphere is due mainly to transport from the stratosphere over North America in the model.

For comparison with previous studies, we use that by Park *et al*. [2004] (hereafter referred to as PK04) because of the large number of flux values provided. Import fluxes

of NOx and NO_y in this study are similar to those from PK04. However, the peak NOx and NOy exports in May in this study are larger than that from PK04 by a factor of 5 and 38%, respectively. In PK04, less CO was exported than imported above 7 km in June; they suggested that the net import of CO is due to a stronger jet stream over the Pacific than over the Atlantic. A similar feature is also found in May in this study. PK04 shows that less O_3 is exported than imported above 9 km in June. By comparison, we find that O_3 export fluxes are similar to the import fluxes in the upper troposphere in May, likely due to higher lightning NOx production in this study.

7.2 Import/export fluxes in the boundary layer and export efficiencies for NOx and NOy

We chose 2.5 km as the top of the boundary layer as in PK04. Table 2 lists the import and export fluxes. For NOx and NOy, export fluxes are larger by a factor of > 10 than import fluxes. The net export is driven mainly by fossil fuel sources. The imports of O_3 and CO show consistent decreasing trends. Decreasing photochemical lifetimes of these species and weakening westerlies from spring to summer reduce the effects of long-range transport. The exports of O_3 and CO also decrease from February to April. In May, the export of both gases increase because of more active convection in REAM, leading to efficient export into the free troposphere. The net exports estimated in REAM for May are similar to the June estimates by PK04 for NOx, NOy, and CO. The export of O_3 in REAM (for May) is lower than PK04 (for June). The reasons are likely two-fold. First, photochemical production is more active in June than in May. Secondly, PK04 used meteorological fields from GEOS-3 Stretched Grid Data Assimilation System (SG-DAS) [Fox-Rabinovitz *et al*., 2002], which may also have deeper mixing depths than MM5

simulations used in REAM, resulting in higher O_3 concentrations near the surface, as in the case of GEOS-CHEM (section 5.2).

North American NOx emissions (20-62°N) are ~1.47 Gmol day^{-1}. About 1.4%, 0.7%, 0.6%, and 0.7% of the emission are exported as NOx, and 20%, 12%, 12%, and 14% are exported as NO_y from the boundary layer from February to May, respectively. The export efficiency of NOx decreases as photochemical oxidations becomes more active during spring. However, more active convection towards May increases the export efficiency. As a result, the simulated export efficiencies do not change much from March to May. REAM estimated NOx export efficiency in May is comparable to that of PK04 (0.6%), but the efficiency for NO_y is twice as large as that of PK04 (7%), suggesting that there may be a large difference between the two models in reactive nitrogen speciation.

5. Conclusions

The spring transitions of O_3, NOx, and CO were characterized based on surface, ozonesonde, aircraft, and satellite measurements over North America from February to May 2000, when rapid photochemical and dynamical changes occur. These observed seasonal changes provide a good testbed to evaluate REAM simulations. The GEOS-CHEM model is used to provide chemical initial and boundary conditions. For illustrations of the effects of key parameters on model simulations, GEOS-CHEM simulations are also used for targeted comparisons with REAM results. The REAM results are generally in good agreement with observations in the troposphere. An exception is the low bias of simulated O_3 concentrations above 350 hPa because the specified upper boundary condition for O_3 (at 100 hPa) is also biased low. The low bias

improves towards the summer and towards lower latitudes as tropospheric photochemical production becomes more dominant.

Fossil fuel NOx emission inventory is evaluated with GOME measurements. Both REAM and GEOS-CHEM products are used in order to test the model dependence of the top-down emission estimates. The monthly top-down estimates differ between the two models for two reasons. First, the different NO_2 profiles lead to 0-12% difference in monthly air mass factors. Second, model differences lead to a different relationship between surface emissions and column NO_2. The resulting monthly top-down emission difference between the two models is 3-20%, in the range of the standard deviation of monthly emission estimates (16-19%) for each model. These differences are averaged out during the 4-month period, leading to close agreement between a priori and top-down emission estimates.

Measurements of tropospheric NOx and O_3 show clear seasonal changes and these changes are captured by REAM simulations. Over the continent, surface NOx and tropospheric column NO_2 decrease despite increasing lightning and soil emissions. Loss by photochemical oxidation of NOx is larger than the source increase. In contrast, tropospheric column NO_2 increases over the western North Atlantic. The increasing trend appears to be due to lightning NO emissions based on REAM results. Monthly mean lightning enhancements are $0.5\text{-}2\times10^{15}$ and $0.5\text{-}1.0\times10^{15}$ molecules cm^{-2} over the continent and western Atlantic, respectively. Some NOx enhancements in May due to lightning and soil emissions are larger than GOME retrieval uncertainties, suggesting that satellite measurements may be used to constrain these emissions.

Surface O_3 over North America increases during spring as photochemistry activates. REAM performs well in simulating the multi-day variations and seasonal transition. In comparison, the rate of surface O_3 increase over the eastern United States in GEOS-CHEM is larger than in REAM (or AIRNow surface observations). A key factor driving the model difference is daytime mixing depth, which is much lower in REAM (simulated by MM5) than it is in GEOS-CHEM (simulated by GEOS-3). With limited supplies of radicals in the springtime, a larger daytime mixing depth in GEOS-CHEM results in faster photochemical activation because radical loss by the reaction of OH and NO_2 is less.

In the free troposphere (400-800 hPa), ozonesonde and MOZAIC measurements show an increase of ~10 ppbv of O_3 from February to May. This increase is well simulated by REAM. Tropospheric O_3 columns derived from TOMS-SAGE II indicate significant increase over the western North Atlantic. Qualitative agreement is found in REAM results, although the simulated magnitudes are lower. Lightning NOx production is found to be the main contributor to the increase of column O_3 over the western North Atlantic.

REAM model simulations are applied to investigate the pollutant imports and exports during spring. Lightning NOx production is a major contributor to the seasonal increase in the exports of NOx and NO_y from North America in the upper troposphere. Simulated NOx export fluxes at 12 km increase by more than a factor of 2 from February to May (1.8 to 4×10^7 moles day^{-1}). In May, lightning production enhances NOx and NO_y exports in the upper troposphere (8-12 km) by 252% and 66%, respectively. In the boundary layer, the import fluxes of O_3 and CO consistently decrease, reflecting a

decrease of long-range transport from spring to summer. The export fluxes of O_3, CO, and NOx from the boundary layer do not exhibit large changes from March to May. The export efficiencies of NOx and NOy from the boundary layer are 0.6-0.7% and 12-14%, respectively.

Acknowledgements. We thank Daniel Jacob and Robert Yantosca for providing GEOS-CHEM model and data, Mian Chin for providing aerosol optical depth data, Dale Allen and Louisa Emmons for helping us analyze MOPITT CO and ozonesonde data, and Kenneth Cummins for providing the NLDN effective detection efficiency. The GEOS-CHEM model is managed at Harvard University with support from the NASA Atmospheric Chemistry Modeling and Analysis Program. This work was supported by the National Science Foundation Atmospheric Chemistry Program.

Appendix. The MOPITT instrument on board the NASA Terra satellite is capable of globally CO monitoring through observations in the thermal band around 4.6 μm. The satellite passes over the equator at around 1045 AM and 2245 PM local time, and the horizontal resolution of MOPITT is 22×22 km^2. During March 2000, the first month when MOPITT data were collected, large amounts of data are missing due to calibrations. We compared REAM results to MOPITT for April and May 2000 (not shown). After processing the model results with the MOPITT averaging kernel [Deeter *et al*., 2003] and considering only the measurements with a priori portion < 60%, we found that the correlation coefficients between simulated and MOPITT monthly mean CO columns are ~0.9 and that the monthly mean bias is ~1%.

References

Allen, D. J., J. E. Dibb, B. Ridley, K. E. Pickering, and R. W. Talbot, An estimate of the stratospheric contribution to springtime tropospheric ozone maxima using TOPSE measurements and beryllium-7 simulations, *J. Geophys. Res., 108(D4)*, 8355, doi:10.1029/2001JD001428, 2003.

Atlas, E. L., B. A. Ridley, and C. Cantrell, The Tropospheric Ozone Production about the Spring Equinox (TOPSE) Experiment: Introduction, *J. Geophys. Res., 108*, 8353, doi:10.1029/2002JD003172, 2003.

Bertram, T. H., et al., Satellite measurements of daily variations in soil NO_X emissions, *Geophys. Res. Lett.*, *32*, L24812, doi:24810.21029/22005GL024640, 2005.

Bey I., D., et al., Global modeling of tropospheric chemistry with assimilated meteorology: Model description and evaluation**,** *J. Geophys. Res., 106*, 23073-23096, 2001.

Black, T. L., The new NMC mesoscale ETA model: Description and forecast examples, *Weather and Forecasting*, *9,* 265-278, 1994.

Cantrell, C. A., et al., Steady state free radical budgets and ozone photochemistry during TOPSE, *J. Geophys. Res.*, *108*, 8361, doi:10.1029/2002JD002198, 2003.

Chance, K., et al., Satellite observations of formaldehyde over North America from GOME, *Geophys. Res. Lett., 27*, 3461-3464, 2000.

Chin, M., et al., Tropospheric aerosol optical thickness from the GOCART model and comparisons with satellite and sunphotometer measurements, *J. Atmos. Sci.*, *59*, 461-483, 2002.

Choi, Y., Y. Wang, T. Zeng, R. Martin, T. Kurosu, and K. Chance, Evidence of lightning NO_x and convective transport of pollutants in satellite observations over North America, *Geophys. Res. Lett., 32,* L02805, doi:10.1029/2004GL021436, 2005.

Deeter, M. N., et al., Operational carbon monoxide retrieval algorithm and selected results for the MOPITT instrument, *J. Geophys. Res.*, *108*(D14), 4399, doi:/4310.1029/2002JD003186, 2003.

Emmons, L. K., et al., Budget of tropospheric ozone during TOPSE from two chemical transport models, *J. Geophys. Res.*, *108*, 8372, doi:10.1029/2002JD002665, 2003.

Environmental Protection Agency (EPA), National air quality and emissions trends report, 1980, 1985, 1989-2000, U. S., Environmental Protection Agency, Research Triangle Park, NC 27111, 2003.

Fox-Rabinovitz, M. S., L. L. Takacs, and R. C. Govindaraju, A variable-resolution ?stretched-grid general circulation model and data assimilation system with multiple areas of interest: Studying anomalous regional climate events of 1998, *J. Geophys. Res., 107*(D24), 4768, doi:10.1029/2002JD002177, 2002.

Geleyn, J. F., Some diagnostics of the cloud/radiation interaction in the ECMWF forecast model. In: Proceedings of Workshop on Radiation and Cloud-Radiation Interaction in Numerical Modeling, pp. 135-162, 1981.

Grell, G. A., Prognostic evaluation of assumptions used by cumulus parameterizations, *Mon. Weather Rev., 121*, 764–787, 1993.

Guillas, S., J. Bao, Y. Choi, and Y. Wang, Downscaling of chemical transport ozone forecasts over Atlanta, *Atmos. Environ.*, in press, 2007.

Herman, J. R., and E. A. Celarier, Earth surface reflectivity climatology at 340-380 nm

from TOMS data, *J. Geophys. Res.*, *102*, 28003-28011, 1997.
Holzworth, G. C., Estimates of mean maximum mixing depths in the contiguous United States, *Mon. Weather Rev*., *92*, 235-242, 1964.
Holzworth, G. C., Mixing Depths, Wind Speeds and Air Pollution Potential for Selected Locations in the United States, *J. Appl. Meteo.*, *6*, 1039-1044, 1967.
Horowitz, L. W., et al., Export of reactive nitrogen from North America during summertime: Sensitivity to hydrocarbon chemistry, *J. Geophys. Res.*, *103*, 13451-13476, 1998.
Jing, P., et al., Isentropic cross-tropopause ozone transport in the Northern Hemisphere, *J. Atmos. Sci.*, *61*, 1068-1078, 2004.
Jing, P., D. Cunnold, Y. Choi, and Y. Wang, Summertime tropospheric ozone columns from Aura OMI-MLS measurements versus regional model results over the United States, *Geophys. Res. Lett.*, *33,* L17817, doi:10.1029/2006GL026473, 2006.
Komhyr, W. D., et al., Electrochemical concentration cell ozonesonde performance evaluating during STOIC 1989, *J. Geophys. Res.*, *100*, 9231-9244, 1995.
Kondo, Y., et al., Photochemistry of ozone over the western Pacific from winter to spring, *J. Geophys. Res.*, *109*(D23), doi:10.1029/2004JD004871, 2004.
Kurosu, T. P., et al., CRAG: Cloud Retrieval Algorithm for the European Space Agency's Global Ozone Monitoring Experiment, in Proceedings of the European Symposium of Atmospheric Measurements From Space, pp. 513-521, Eur. Space Agency, Paris, 1999.
Lamarque, J.-F., and P. G. Hess, Model analysis of the temporal and geographical origin of the CO distribution during the TOPSE campaign, *J. Geophys. Res., 108(D4),* 8354, doi:10.1029/2002JD002077, 2003.
Liang, J., et al., Seasonal budgets of reactive nitrogen species and ozone over the United States, and export fluxes to the global atmosphere, *J. Geophys. Res.*, *103*, 13435-13450, 1998.
Marenco, A., et al., Measurement of ozone and water vapor by Airbus in-service aircraft: The MOZAIC airborne program, An overview, *J. Geophys. Res.*, *103*, 25631-25642, 1998.
Martin, R. V., et al., An improved retrieval of tropospheric nitrogen dioxide from GOME, *J. Geophys. Res., 107*(D20), 4437, doi:4410.1029/2001JD001027, 2002.
Martin, R. V., et al., Global inventory of nitrogen oxide emissions constrained by space-based observations of NO_2 columns, *J. Geophys. Res., 108*(D17), 4537, doi:4510.1029/2003JD003453, 2003.
National Research Council (NRC), Rethinking the Ozone Problem in Urban and Regional Air Pollution, Natl. Acad., Washington D. C., 1991.
Park, R. J., et al., Global simulation of tropospheric ozone using the University of Maryland Chemical Transport Model (UMD-CTM): 2. Regional transport and chemistry over the central United States using a streched grid, *J. Geophys. Res.*, *109*, D09303, doi:09310.01029/02003JD004269, 2004.
Price, C., et al., NO_X from lightning 1. Global distribution based on lightning physics, *J. Geophys. Res.*, *102*(D5), 5929-5941, 1997.
Price, C., Evidence for a link between global lightning activity and upper tropospheric water vapor, *Nature*, *406*, 290-293, 2000.

Price, C., and D. Rind, Modeling global lightning distributions in a general circulation model, *Mon. Weather Rev., 122*, 1930-1939, 1994.
Rind, D., Just add water vapor, *Science*, *281*, 1152-1153, 1998.
Spurr, R. J. D., et al., A linearlized discrete ordinate radiateive transfer model for atmospheric remote sensing retrieval, *J. Quant. Spectrosc. Radiat. Transfer*, *68*, 689-735, 2001.
Stauffer, D. R., et al., Use of four-dimensional data assimilation in a limited-area mesoscale model part II. Effects of data assimilation within the planetary boundary layer, *Mon. Weather Rev., 119*, 734-754, 1991.
Stephens, G., et al., Radiation profiles in extended water cloud III: Obsrevations, *J. Atmos. Sci.*, *35*, 2133-2141, 1978.
Thouret, V., et al., Ozone climatologies at 9-12 km altitude as seen by the MOZAIC airborne program between September 1994 and August 1996, *J. Geophys. Res.*, *103*, 25653-25679, 1998.
Thouret, V., et al., Tropopause referenced ozone climatology and inter-annual variability (1994-2003) from the MOZAIC programme, *Atmos. Chem. Phys.*, *6*, 1033-1051, 2006.
Walcek, C. J., Minor flux adjustment near mixing ratio extremes for simplified yet highly accurate monotonic calculation of tracer advection, *J. Geophys. Res.*, *105*, 9335–9348, 2000.
Wang, H.-J., et al., Assessment of SAGE version 6.1 ozone data quality, *J. Geophys. Res.*, *107*, 4691, doi:10.1029/2002JD002418, 2002.
Wang, H.-J., et al., SAGE III solar ozone measurements: Initial results, *Geophys. Res. Lett.*, *33*, L03805, doi:03810.01029/02005GL025099, 2006.
Wang, Y., et al., Global simulation of tropospheric O_3-NO_X-hydrocarbon chemistry: 1. Model formulation, *J. Geophys. Res.*, *103*, 10713-10725, 1998.
Wang, Y., et al., Springtime photochemistry at northern mid and high latitudes, *J. Geophys. Res.*, *108*, 8358, doi:10.1029/2002JD002227, 2003a.
Wang, Y., et al., Intercontinental transport of pollution manifested in the variability and seasonal trend of springtime O3 at northern mid and high latitudes, *J. Geophys. Res., 108,* D21, 4683, 10.1029/2003JD003592, 2003b.
Wang, Y., Y. Choi, T. Zeng, B. Ridley, N. Blake, D. Blake, and F. Flocke, Late-spring increase of trans-Pacific pollution transport in the upper troposphere, *Geophys. Res. Lett.*, *33*, L01811, doi:10.1029/2005GL024975, 2006.
Wang, Y., Y. Choi, T. Zeng, D. Davis, M. Buhr, G. Huey, and W. Neff, Assessing the photochemical impact of snow NO_X emissions over Antarctica during ANTCI 2003, *Atmos. Env.*, *Atmos. Environ.*, *41,* 3944-3958, 2007.
Yienger, J. J., and H. Levy II, Empirical model of global soil-biogenic NO_X emissions, *J. Geophys. Res.*, *100*, 11447-11464, 1995.
Zeng, T., et al., Widespread persistent near-surface ozone depletion at northern high latitudes in spring, *Geophys. Res. Lett.*, *30*, 2298, 10.1029/2003GL018587, 2003.
Zeng, T., et al., Halogen-driven low altitude O_3 and hydrocarbon losses in spring at northern high latitudes, *J. Geophys. Res.*, *111*, D17313, doi:10.1029/2005JD006706, 2006.

Table 1. Monthly North America (20 - 62°N) fossil fuel NO_X emissions (Tg N $month^{-1}$)

	REAM derived			GEOS-CHEM derived		
	A priori	Top-down	A posteriori	A priori	Top-down	A posteriori
February	0.57	0.49	0.52	0.55	0.41	0.47
March	0.61	0.76	0.69	0.61	0.66	0.64
April	0.59	0.66	0.63	0.58	0.64	0.61
May	0.61	0.59	0.60	0.60	0.71	0.66
Average	0.60	0.63	0.61	0.59	0.61	0.60

Table 2. Import and export fluxes of pollutants in the boundary layer (<2.5 km) over North America (20 – 62°N, Gmol day^{-1})

	Import fluxes				Export fluxes			
	Feb	Mar	Apr	May	Feb	Mar	Apr	May
NO_x	$< 10^{-4}$	$< 10^{-4}$	$< 10^{-4}$	$< 10^{-4}$	0.02	0.01	0.01	0.01
NO_y	0.01	0.02	0.02	0.01	0.31	0.20	0.19	0.21
CO	18	17	13	9	33	19	14	16
O_3	5.2	4.5	3.8	2.5	8.2	5.2	4.2	5.3

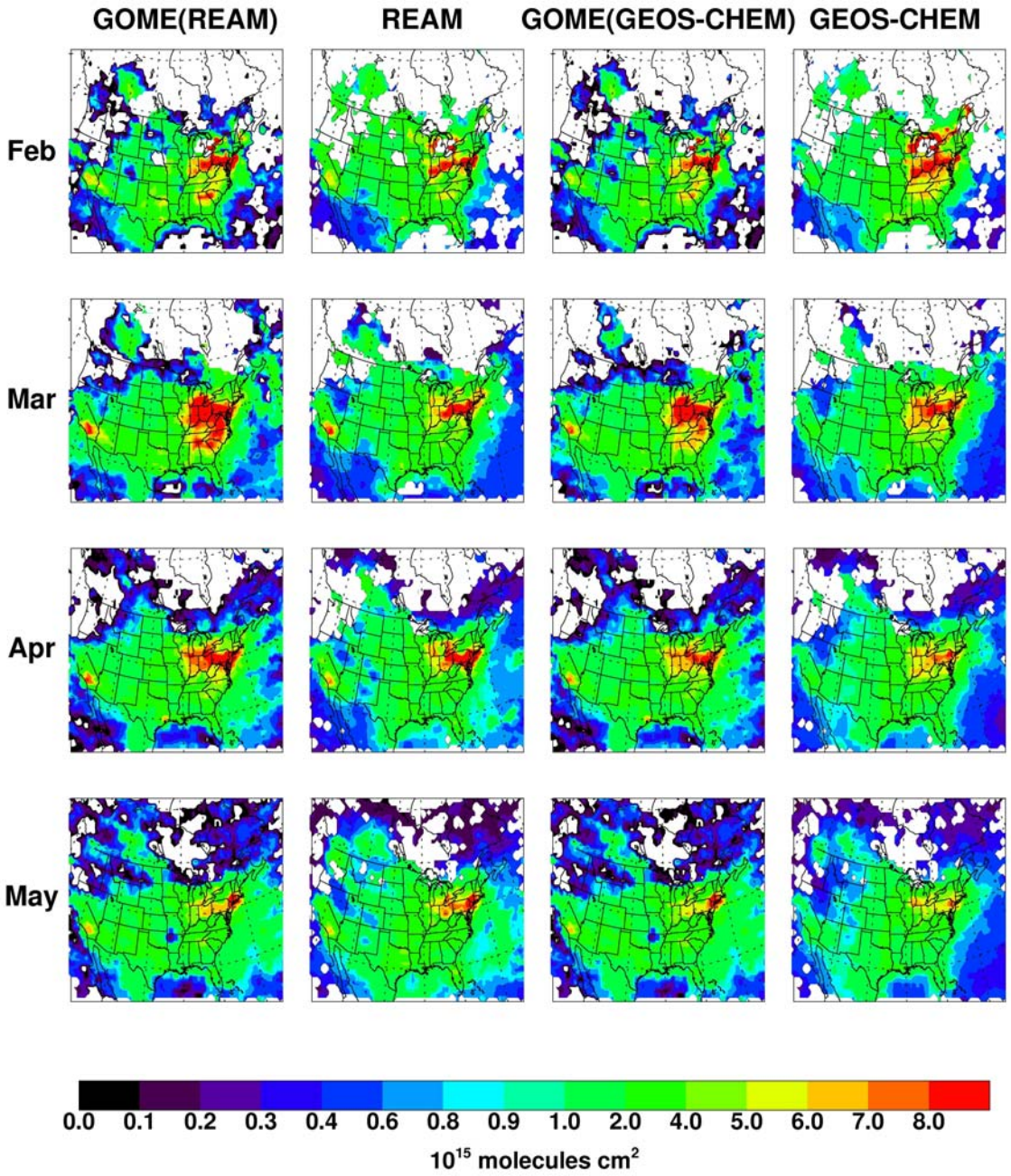

Figure 1. Monthly mean tropospheric NO_2 vertical columns during February-May 2000 from GOME retrievals using the REAM-derived shape factor (first column), the REAM model (second column), GOME retrievals using the GEOS-CHEM-derived shape factor (third column), and the GEOS-CHEM model (last column). Only measurements with cloud fraction ≤ 40% are used. The text provides the description of retrieval process. The model results are obtained by averaging NO_2 data during the satellite overpass time period (1000-1100, LT).

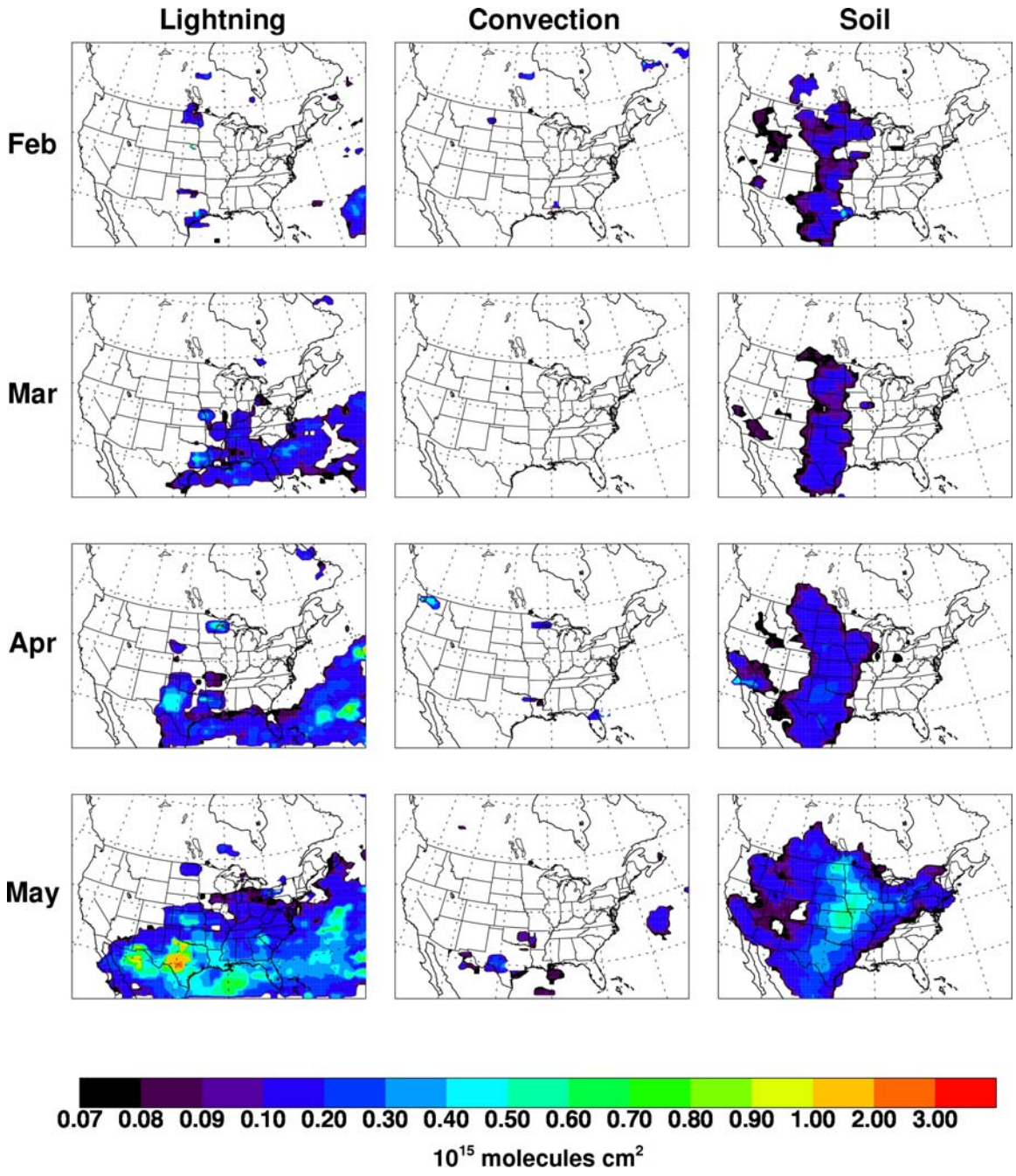

Figure 2. Monthly mean contributions of lightning production, convection, and soil emissions to tropospheric NO_2 vertical columns.

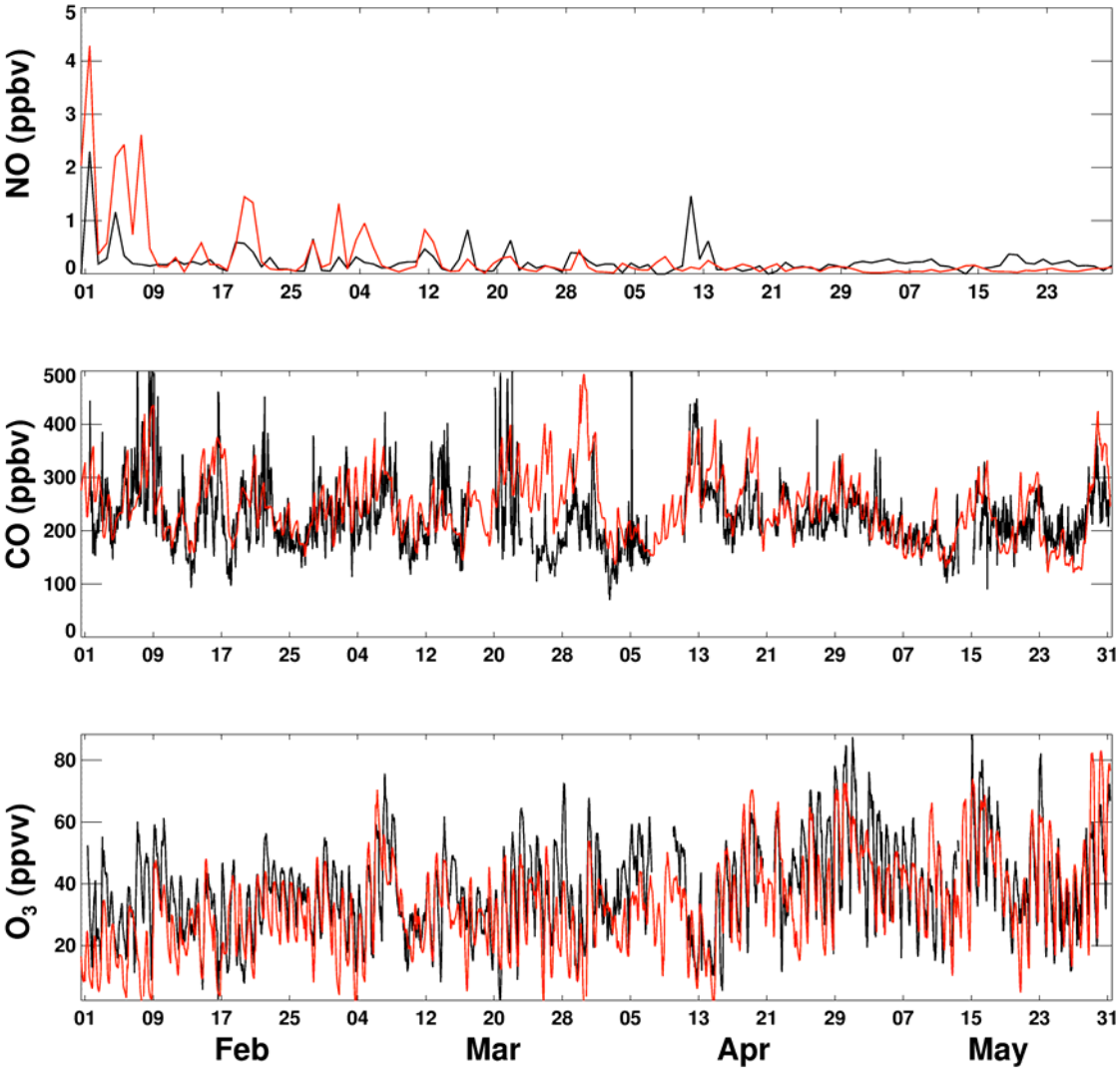

Figure 3. Observed and simulated afternoon (1300-1700 LT) average NO, and hourly CO and O_3 at the Oak Grove site (89° W, 32° N). The solid black lines represent the SEARCH measurements and red lines represent the REAM results.

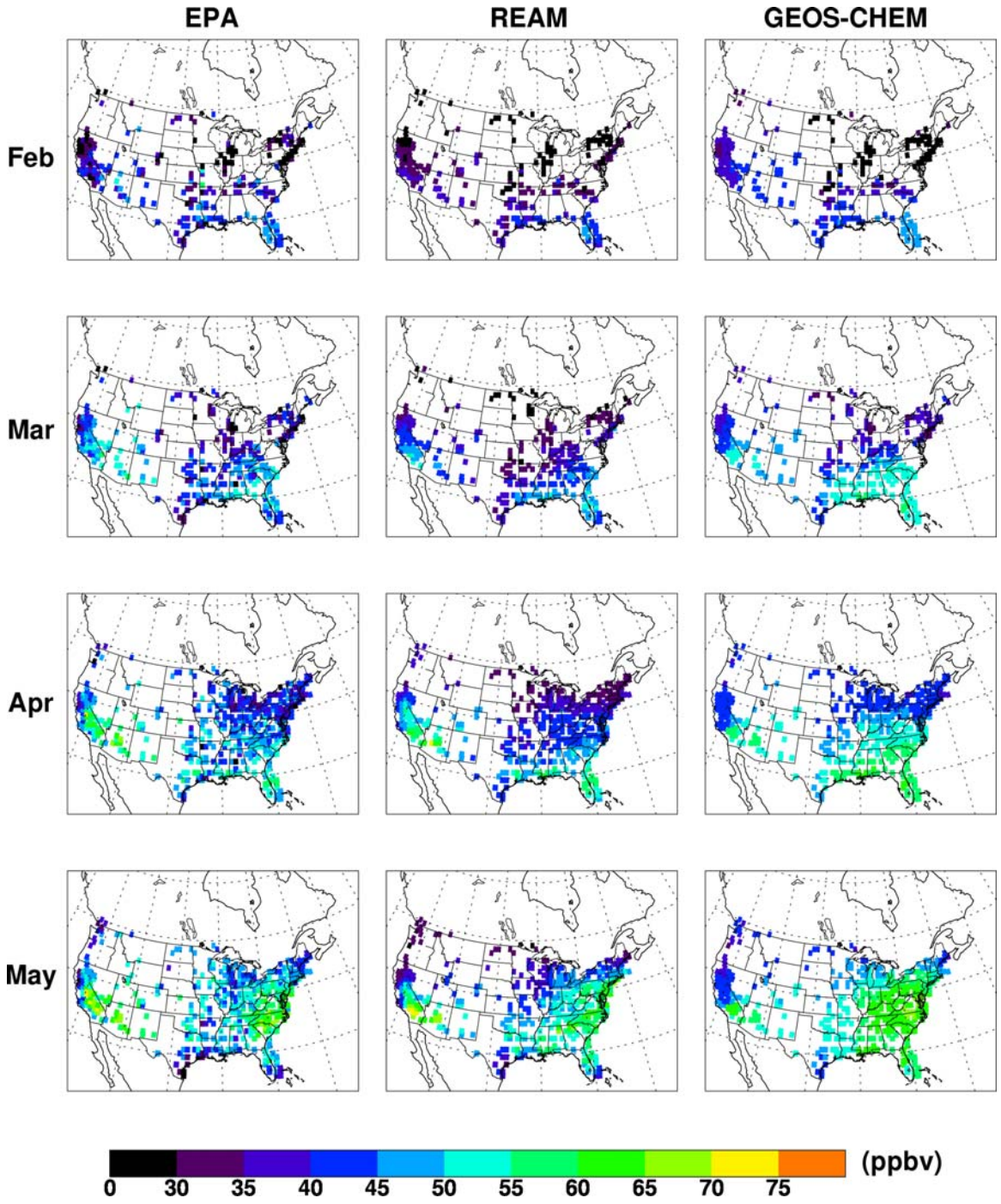

Figure 4. Monthly mean afternoon (1300-1700, LT) surface O_3 concentrations (ppbv) over the United States in February-May 2000. Shown are the EPA AIRNow observations at rural sites (left column), REAM simulation results (middle column), and GEOS-CHEM simulation results (right column).

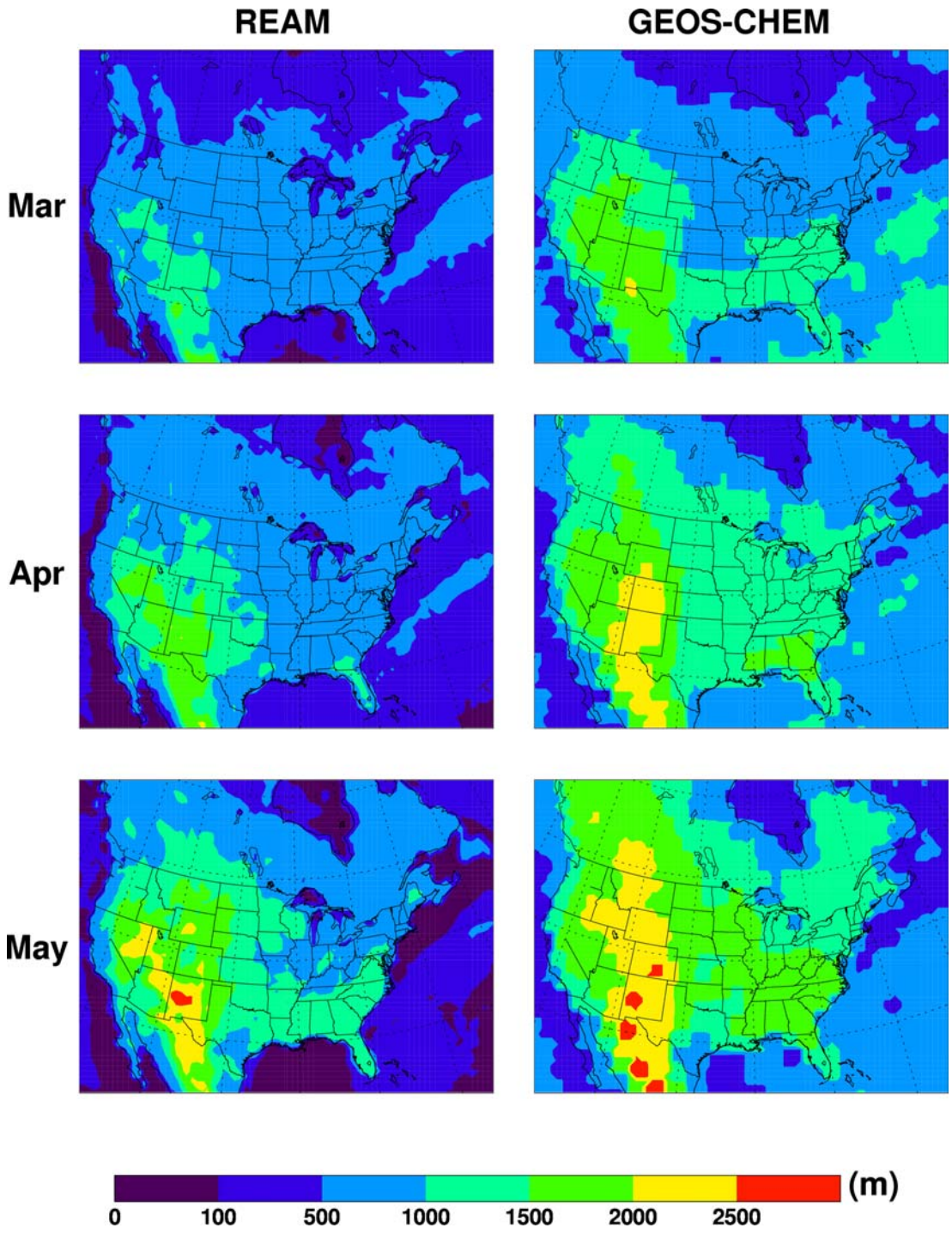

Figure 5. Average afternoon (1200-1600, LT) mixing depths over North America in March-May 2000. The data used in REAM (left column) are simulated by MM5, and those used in GEOS-CHEM (right column) are simulated by GEOS-3.

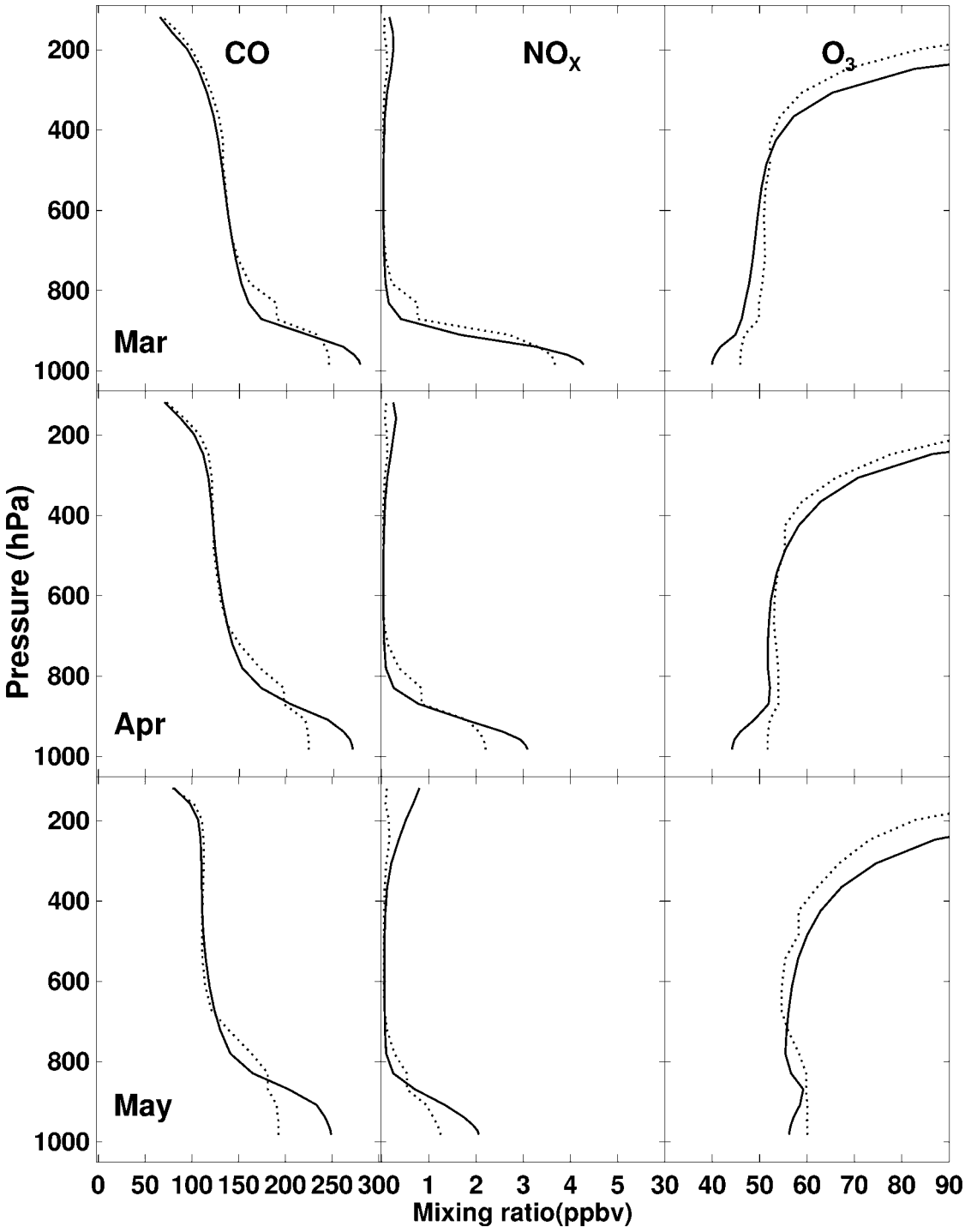

Figure 6. Comparisons of monthly averaged afternoon (1200-1600, LT) vertical profiles of CO, NOx, and O_3 concentrations between REAM and GEOS-CHEM models. The profile is averaged over the continental region of 75-90° W and 30-42° N. The solid lines represent the REAM simulations, and the dotted lines represent the GEOS-CHEM simulations.

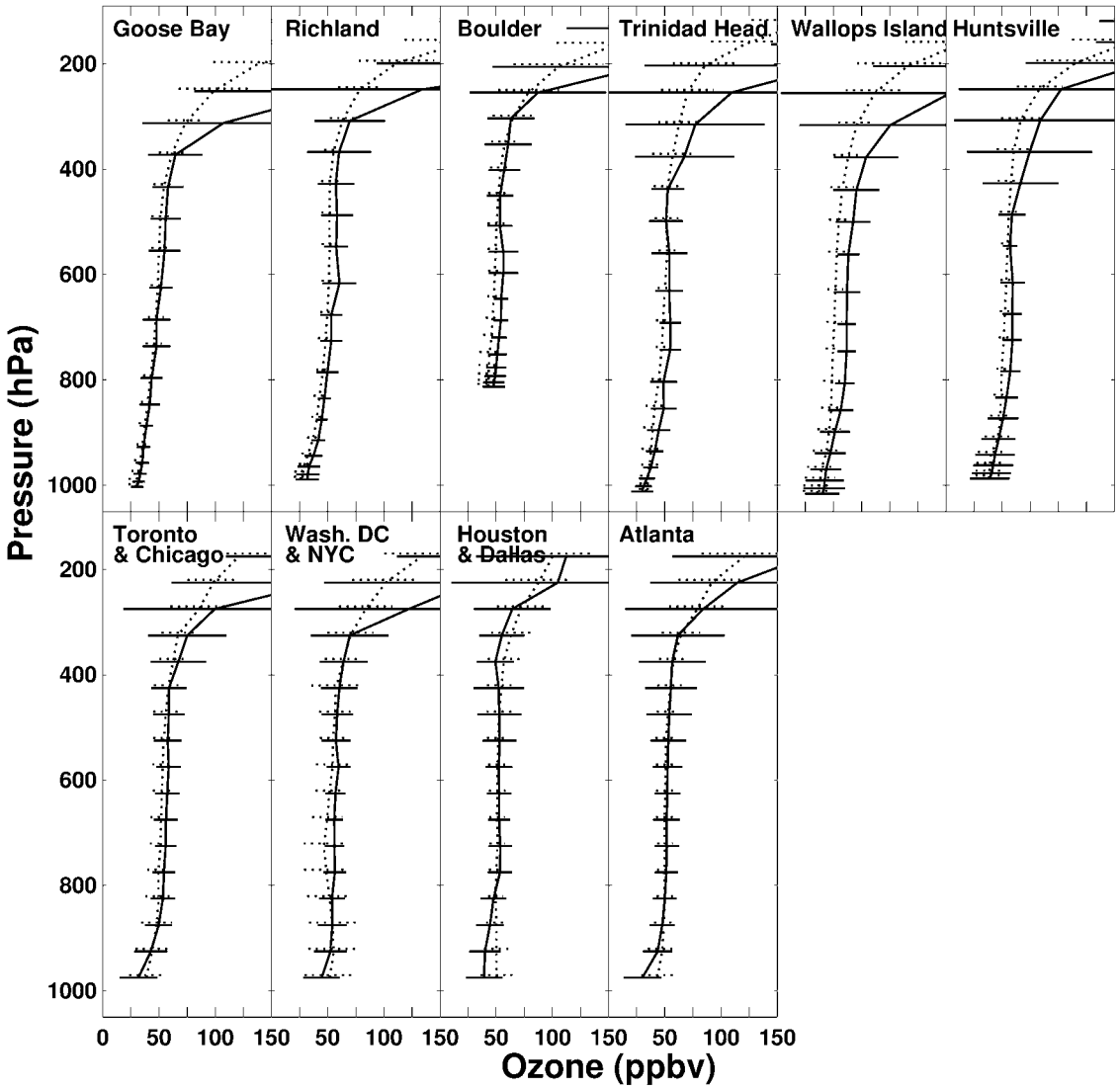

Figure 7a. Observed and simulated mean O_3 profiles for February-May, 2000. The upper and lower panels show the observations from ozonesondes and MOZAIC program in solid lines, respectively. Horizontal bars show standard deviations. Dotted lines show corresponding REAM results. The ozonesonde sites include: Goose Bay (53° N, 60° W), Richland (46° N, 119° W), Boulder (40° N, 105° W), Rinidad Head (41° N, 124° W, Wallops Island (38° N, 75° W), and Hunsville (35° N, 87° W). "Wash. DC" denotes Washington, DC and "NYC" denotes New York City.

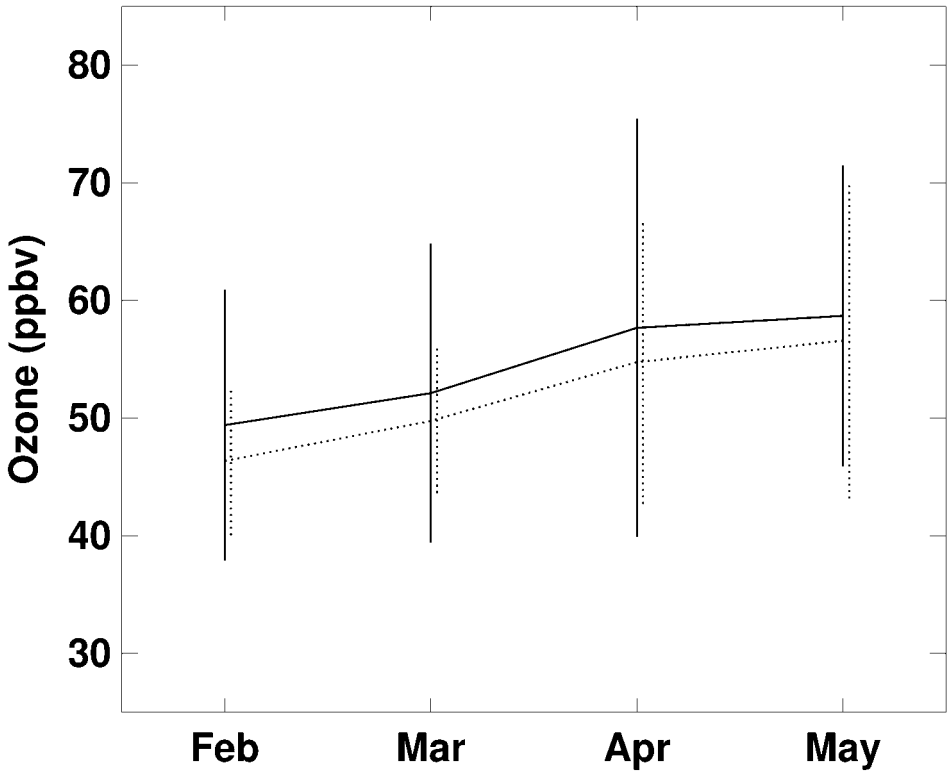

Figure 7b. Observed and simulated monthly tropospheric O_3 mixing ratios at 400-800 hPa. The solids lines show means and standard deviations of ozonesonde and MOZIAC measurements. The dotted lines show corresponding REAM results.

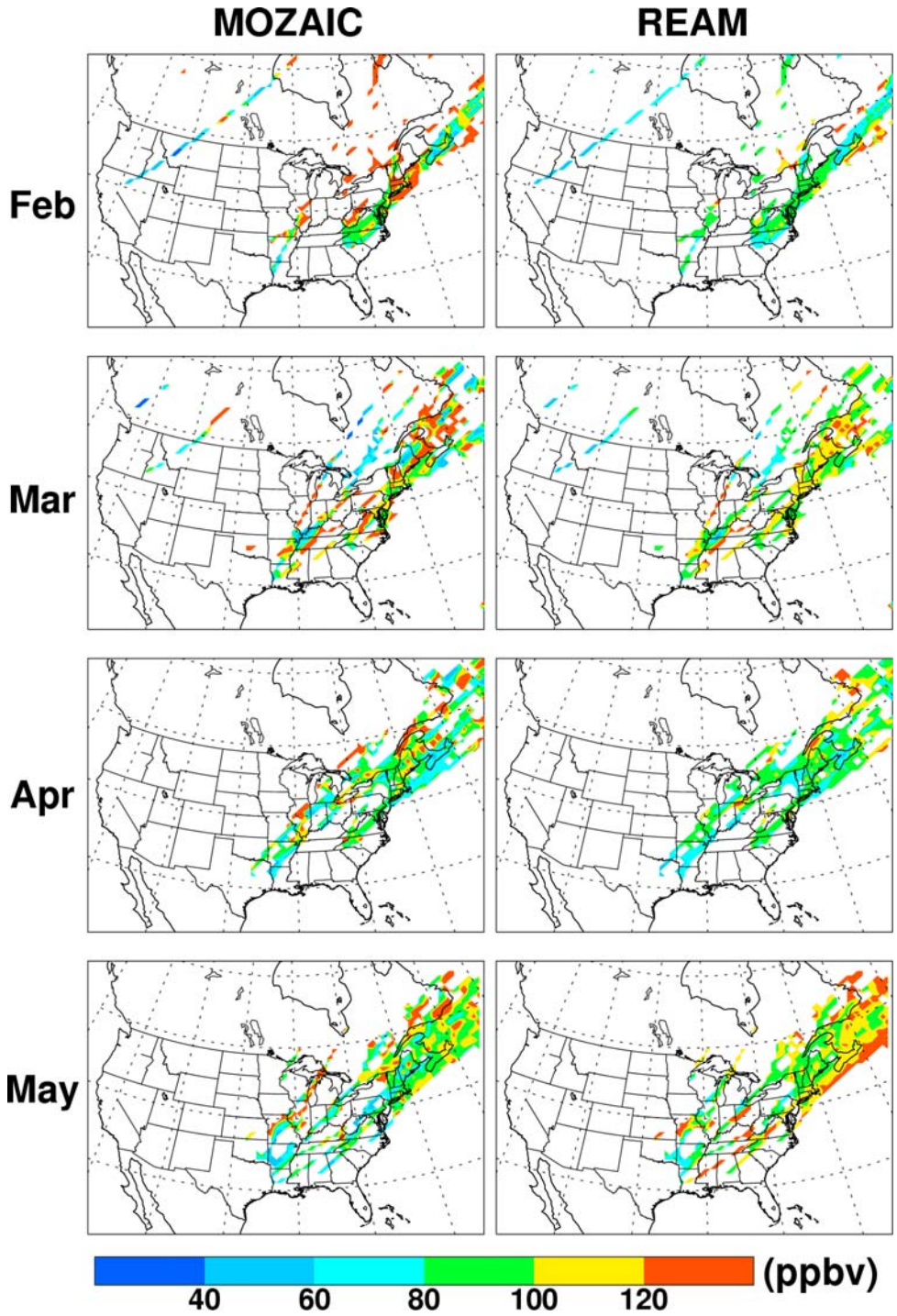

Figure 8. Mean O_3 concentration (ppbv) at 150-250 hpa from the MOZAIC measurements during February-May 2000 (left column) and the corresponding REAM results (right column). REAM data are sampled along MOZAIC aircraft tracks. Ozone data > 200 ppbv from MOZAIC and REAM are filtered out.

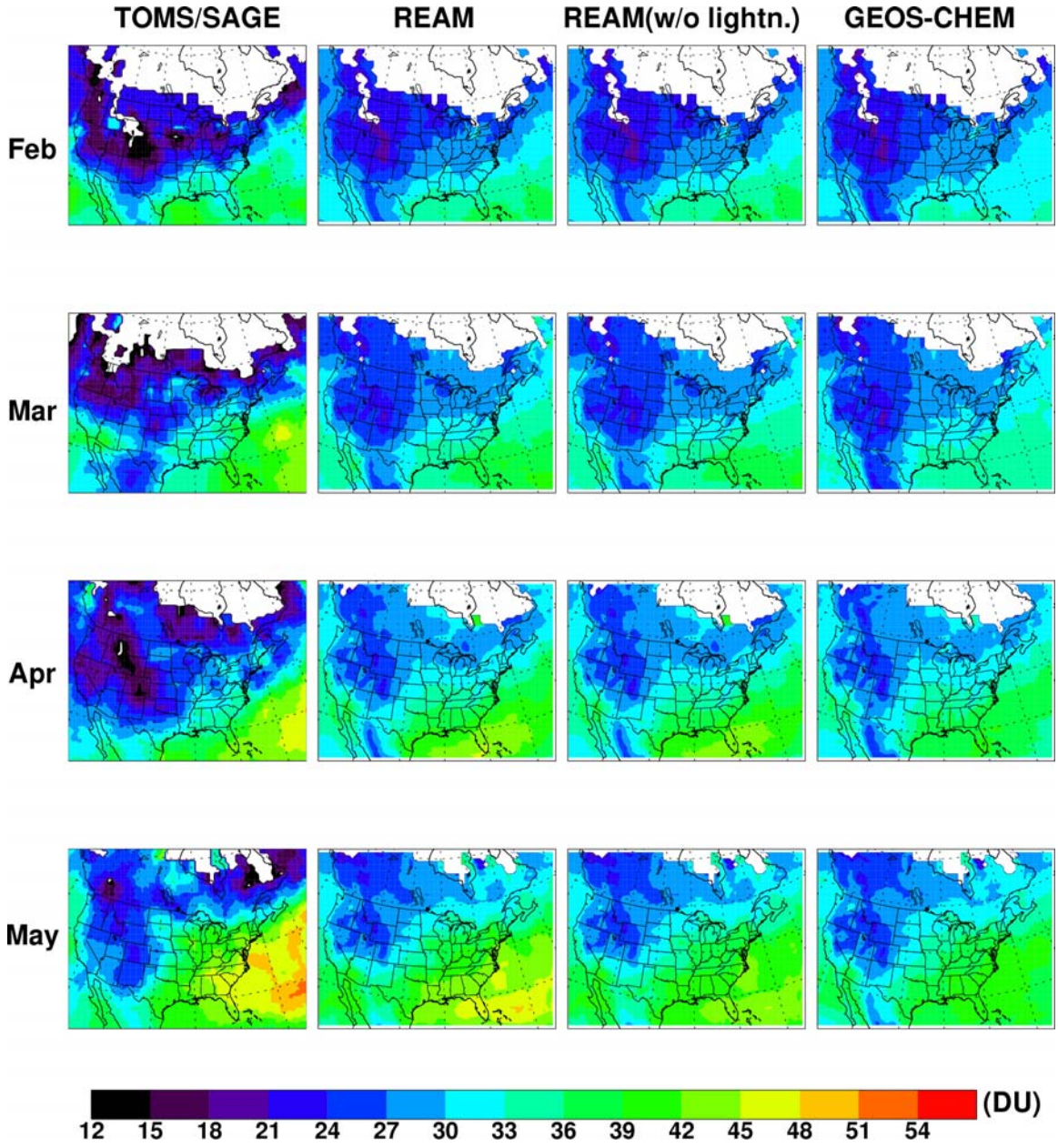

Figure 9. Monthly mean tropospheric O_3 columns derived from TOMS total columns and SAGE II stratospheric columns (first column), the REAM standard simulation (second column), the REAM sensitivity simulation without lightning NO_X production (third column), and the GEOS-CHEM simulation (last column).

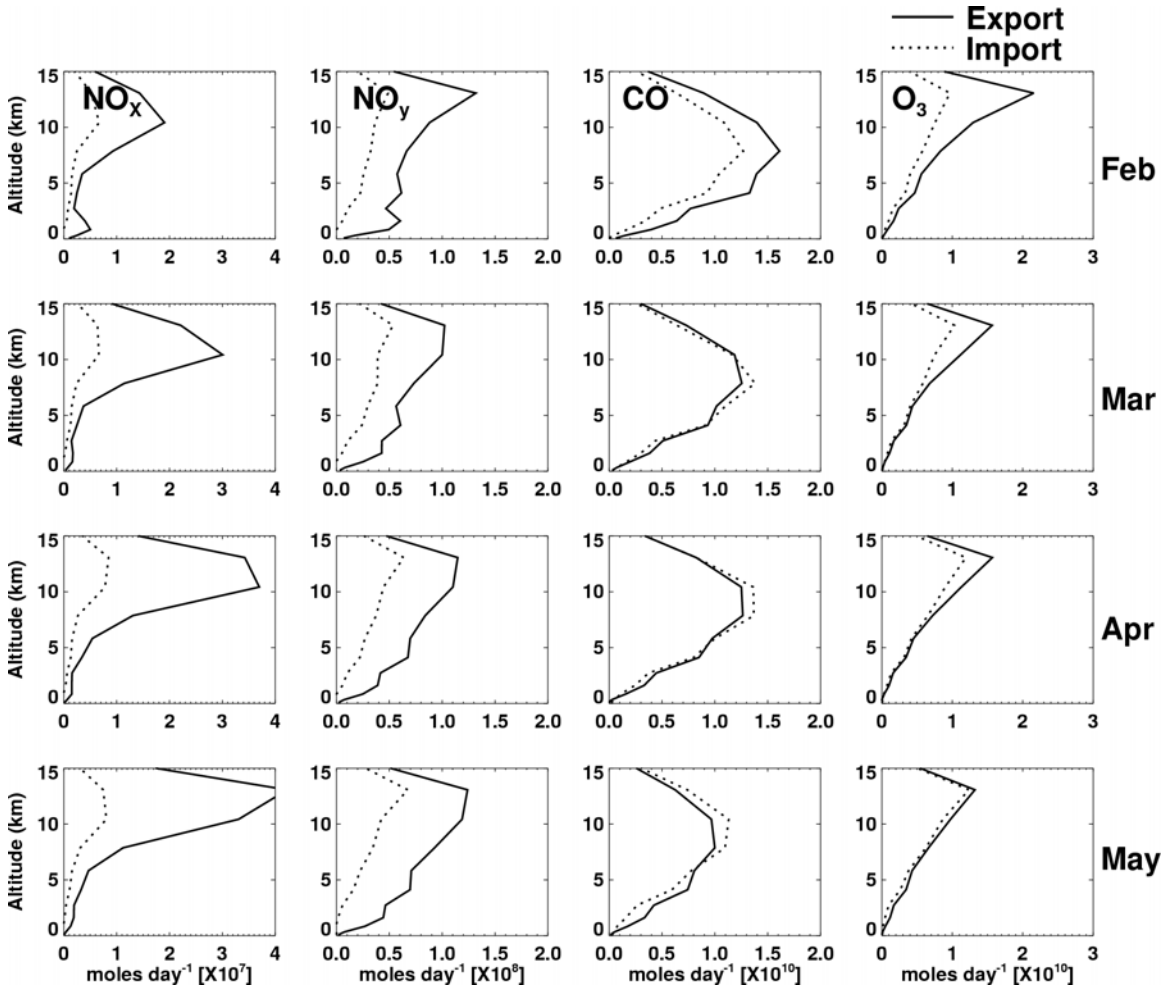

Figure 10. Vertical profiles of longitudinal import and export fluxes of NO_X, NO_y, CO, and O_3 over North America in the troposphere. The western and eastern boundaries are the same as those depicted in Figure 10. The solid lines represent export fluxes while the dotted lines represent import fluxes.